Raman-active modes in finite and infinite double-walled carbon nanotubes

A. Rahmani*
Département de Physique, Université My Ismail, Faculté des Sciences, BP 4010, 50000 Meknès, Morocco

J.-L. Sauvajol, J. Cambedouzou, and C. Benoit
Groupe de Dynamique des Phases Condensées (UMR CNRS 5581), Université Montpellier II, 34095 Montpellier Cedex 5, France
(Received 3 May 2004; revised manuscript received 2 September 2004; published 10 March 2005)

The calculation of the nonresonant Raman spectrum of double-walled carbon nanotubes (DWCNT's) is performed in the framework of the bond polarization theory, using the spectral moment method. The calculation of the Raman spectrum of DWCNT's as a function of the diameter and chirality of the inner and outer tubes allows us to derive the diameter dependence of the frequencies of the breathing-like modes (BLM's) and tangential-like modes (TLM's) in a large diameter range. In particular, the diameter dependence of the frequencies of the two radial breathing-like modes (RBLM's) resulting from the in-phase and counterphase coupled motions of the totally symmetric radial breathing mode (the so-called RBM) of the inner and outer tubes is discussed. The Raman spectrum of a bundle of identical DWCNT's is also calculated. The dependence of the spectrum with the size of the bundle is analyzed. Additional breathing-like modes are predicted in DWCNT bundles of finite size. The majority of these peaks rapidly vanish when the tube length increases, except a totally symmetric mode that subsists in the DWCNT crystal.

DOI: 10.1103/PhysRevB.71.125402 PACS number(s): 78.30.Na, 61.48.+c, 63.22.+m

I. INTRODUCTION

Recently, double-wall carbon nanotubes (DWCNT's), which consist of two concentric cylindrical graphene layers, have been successfully synthesized by catalytic chemical vapor deposition[1–3] and by the thermal conversion of C_{60} encapsulated in single-wall carbon nanotubes (SWCNT's).[4] Double-wall carbon nanotubes are the subject of intense studies due to their promising applications. In particular, the DWCNT with a metallic inner tube and an insulating outer tube is a model system for a molecular conductive wire covered by an insulator.

Raman scattering is a useful technique to study the one-dimensional properties of carbon nanotubes, since it can probe both the phonon spectrum and the electronic structure.[5] In past years, Raman scattering investigations mostly focused on SWCNT's (for a review on Raman results in bundled and isolated SWCNT's, see Refs. 6–8). To derive this information, the Raman data have to be correlated to theoretical predictions, and different approaches have been developed.[8–12] Recently, we used the spectral moment method in the framework of the bond-polarization theory to calculate polarized nonresonant Raman spectra of chiral and achiral SWCNT's as a function of their diameter and length.[13]

Recently, Raman experiments on DWCNT's have been performed. The data were mostly analyzed on the basis of the theoretical predictions stated for SWCNT's. A detailed Raman investigation of DWCNT's prepared from thermal conversion of C_{60} encapsulated in SWCNT's has been recently reported.[4,14] The Raman spectra have been measured using 488.0, 514.5, 647.1, and 1064 nm excitation wavelengths. These authors use the linear relation between the frequency of the totally symmetric radial breathing model (the so-called RBM) and the inverse of the diameter, found in SWCNT's,

$$\omega_{RBM} = A/D, \tag{1}$$

to assign the different pairs of inner and outer tubes present in their samples. In this attribution, the diameter D of the previous expression is D_{inner} for the inner tube and D_{outer} for the outer tube with $D_{outer}=D_{inner}+2d$, where d is the distance between the inner and outer tubes. It is fixed at $\approx$3.4 Å in agreement with the interlayer spacing of graphite (3.4 Å). In SWCNT's, the prefactor A is known to be model dependent and the following values have been predicted: $A=223$ cm^{-1} nm,[8] 234 cm^{-1} nm,[10] 236 cm^{-1} nm,[11] 227 cm^{-1} nm,[12] and 225 cm^{-1} nm.[13] In their assignment, neglecting the tube-tube interaction, these authors take the average value for A, namely $A=234$ cm^{-1} nm.

The Raman spectra measured on samples prepared by the catalytic chemical vapor deposition (CCVD) method have been recently reported.[15] In this study also, the linear relation between the RBM frequency and the inverse of diameter is assumed to be relevant. The difference between experimental and predicted RBM frequencies is understood in terms of the reduced interlayer distance between the inner and the outer tubes due to the tube-tube interaction (d is assumed to range from 2.97 to 3.4 Å).

More recently, DWCNT's prepared by the floating catalyst CVD method were studied by Raman scattering.[16] The assignment of the inner tube and outer tube is done according to the following assumptions: (i) the interlayer spacing between the inner and the outer tubes increases as the tube diameter decreases—the smaller the diameter, the larger the interlayer spacing, following the equation $2d=0.688+0.2\exp(-D_{inner}/2)$, (ii) the diameters of the tubes are derived from the experimental frequencies of the totally symmetric breathing mode by using the equation $\omega_{RBM}=238/D^{0.93}$, which was found to relate the RBM frequency and the tube diameter in the SWCNT bundle (this

latter expression takes into account the tube-tube interaction).[17] A reasonable agreement between experimental and calculated frequencies is found, which allows authors to assign the chirality pairs of inner and outer tubes of different DWCNT's.

It was found that the linear relation between the RBM frequency and the inverse of diameter requires a correction in SWCNT bundles[17–20] as well as in multiwalled carbon nanotubes.[21] The main reason is that the tube-tube interactions cannot be neglected in these nanostructures. In DWCNT the in-phase and counterphase coupling between the breathing modes of the inner and outer tubes leads to collective breathing-like modes (BLM's).[21,22] Obviously, the van der Waals interaction between the tubes has to be taken into account to describe these modes.

In this paper we present calculations of the nonresonant Raman spectrum of DWCNT's in the breathing-like mode (BLM) and tangential-like mode (TLM) ranges. These calculations have been performed in the framework of the nonresonant bond-polarization theory using the spectral moment method (SMM).[13,23] It is obvious that the Raman intensity calculated by this nonresonant method cannot match the experimental spectra, which display a strong resonant character in carbon nanotubes. Nevertheless, the SMM predictions concerning the number and frequencies of Raman active lines as a function of diameter, length, and chirality do not depend on the resonant process of Raman scattering. In consequence, the SMM predictions can help to interpret the frequencies of the Raman active modes. After a brief description of the method used to compute the Raman spectra, we present the results obtained on isolated DWCNT's of infinite and finite lengths, and on DWCNT bundles of different sizes.

II. COMPUTATIONAL METHOD

In the DWCNT's under consideration, the inner and outer tubes are assumed to be at a distance d close to 3.4 Å ± 10%, and the relation between the diameters of the inner (D_{inner}) and outer (D_{outer}) tubes is $D_{outer}=D_{inner}+2d$. On the other hand, the diameter of a (n,m) carbon nanotube is given by $D=a[3(m^2+mn+n^2)]^{1/2}/\pi$, with $a=1.42$ Å. The previous relations allow us to derive all the possible (k,l) outer tubes for a specific (n,m) inner tube, which lead to $(n,m)@(k,l)$ DWCNT's. For instance, the $(n,n)@(n+5,n+5)$ DWCNT's satisfy the previous conditions.

In order to form a homogeneous bundle, the DWCNT's are placed parallel to each other on a finite-size hexagonal array of cell parameter $a_0=D_{out}+d_{t-t}$, with the DWCNT-DWCNT spacing d_{t-t} fixed to 3.2 Å. The number of DWCNT's per bundle is N_t. Except for the dimer ($N_t=2$), the number of tubes is such that the DWCNT's form complete concentric shells (in consequence, N_t is 7,19,37).

The C-C intratube interactions are described by using the same force constant set as the one used in our calculation of the Raman spectrum of isolated single-wall carbon nanotubes.[13] A Lennard-Jones potential, $U_{LJ}=4\epsilon[(\sigma/R)^{12}-(\sigma/R)^6]$, is used to describe the van der Waals intertube interactions between inner and outer tubes in DWCNT's as well as between the DWCNT's in bundle. The values of the Lennard-Jones parameters are kept fixed at $\epsilon=2.964$ meV and $\sigma=3.407$ Å.[13]

We calculate the Raman spectra for isolated DWCNT's and DWCNT bundles of finite and infinite lengths using the SMM.[23] For SWCNT's, the SMM method is described in detail in Ref. 13 and the same approach is used in this work. The polarizability Raman tensor of each vibrational mode is calculated in the framework of the nonresonant bond-polarizability model.[24] The frequencies of the Raman-active modes are derived from the position of the peaks in the calculated Raman spectra (the linewidth of each peak was fixed at 1.7 cm^{-1}). The intensity of the Raman spectrum is normalized with respect to the number of carbon in the sample under consideration. In our calculations, the common axis of the inner and outer tubes is along the Z axis, and a carbon atom of each tube is along the X axis of the DWCNT reference frame. The laser beam is kept along the y axis of the reference frame. The polarized ZZ, ZX, and XY Raman spectra on one hand, and the VV spectrum (both the incident and scattered polarizations along the z axis) corresponding to an isotropic distribution of the DWCNT orientation (powder sample) on the other hand, are calculated.

III. RESULTS

In this section, we report the calculated Raman spectra for infinite and finite isolated DWCNT's and for DWCNT bundles of different sizes. The dependence of the Raman spectrum as a function of tube diameter and chirality is investigated. We calculate the Raman spectra of different achiral@achiral, chiral@chiral, achiral@chiral, and chiral@achiral DWCNT's.

A. The Raman spectrum of isolated DWCNT's

For different DWCNT's the Lennard-Jones intertube interaction energy was minimized with respect to the interlayer separation, the relative angle of rotation of the layers around the tube axis, and their relative translation along the tube axis. The optimal intertube gap is found around 3.4 Å. Calculations of the Raman spectra, before and after energy minimization, do not show significative difference in the mode frequencies. This result is in agreement with that of Popov and Henrard,[21] who found no significant differencies between the BLM and TLM frequencies of the optimized and nonoptimized DWCNT's in terms of relative angles of rotation and relative translations of the inner and outer tubes. For infinite DWCNT's, calculations are performed by applying periodic conditions on unit cells.

In a first part, we focus on the Raman spectra of armchair@armchair DWCNT. These DWCNT's are identified as $(n,n)@(n+5,n+5)$. In order to illustrate our results, the calculated Raman spectra of (5,5)@(10,10), (7,7)@(12,12), and (10,10)@(15,15) DWCNT's are shown in the BLM (Fig. 1, top) and TLM (Fig. 1, bottom) ranges, respectively.

In the BLM range, VV Raman spectrum shows six modes resulting from the in-phase and counterphase coupled motions of the breathing modes of the inner and outer tubes. In

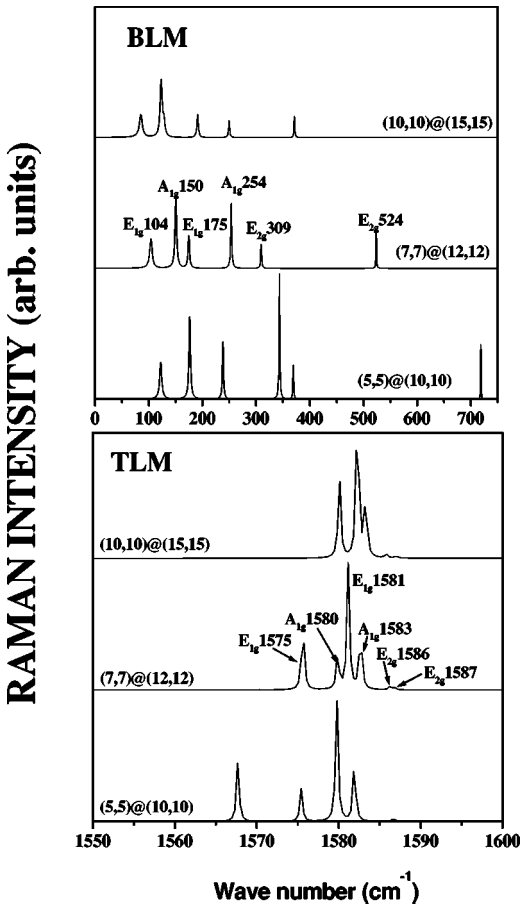

FIG. 1. The calculated Raman spectra of infinite (5,5)@(10,10), (7,7)@(12,12), and (10,10)@(15,15) DWCNT's in the BLM (top) and TLM (bottom) regions.

the *ZZ*, *ZX*, and *XY* polarized spectra, a pair of lines are systematically calculated. The same behavior was found in SWCNT's where a single A_{1g} mode is observed in the *ZZ* spectrum, a single E_{1g} mode is active in the *ZX* spectrum, and a single E_{2g} mode in the *XY* spectrum.[13] For simplicity, we assign the BLM of DWCNT's from the symmetry of the breathing modes of SWCNT's measured in the same polarized spectrum. For example, in Fig. 1, the Raman spectrum of the (7,7)@(12,12) DWCNT displays peaks located at 254 and 150 cm^{-1} (A_{1g}), 175 and 104 cm^{-1} (E_{1g}), and 524 and 309 cm^{-1}(E_{2g}). The frequencies of the breathing modes in isolated (7,7) and (12,12) armchair tubes are calculated at 235 and 137 cm^{-1} (A_{1g}), 166 and 98 cm^{-1} (E_{1g}), and 521 and 306 cm^{-1}(E_{2g}). Then, our calculations state a systematic upshift of the frequencies of the BLM's with respect to the frequencies of the breathing modes in SWCNT's. Figure 2 displays the relation between the BLM frequencies and the diameter of the outer tube, D_{outer}, in $(n,n)@(n+5,n+5)$ DWCNT's. A downshift of all the BLM's is found when the diameter increases.

We focus now on the dependence with the diameter of the specific breathing-like modes that results from the in-phase and counterphase coupled motions of the RBM's (A_{1g} symmetry) of the inner and outer tubes. These modes are called RBLM's in the following. For several DWCNT's, the eigenvectors of modes were obtained from the direct diagonalization of the dynamical matrix (infinite DWCNT's). By using these results, we found that the in-phase motion of both tubes is associated with the low-frequency RBLM's and the counterphase motion of both tubes is related to the high-frequency RBLM's.

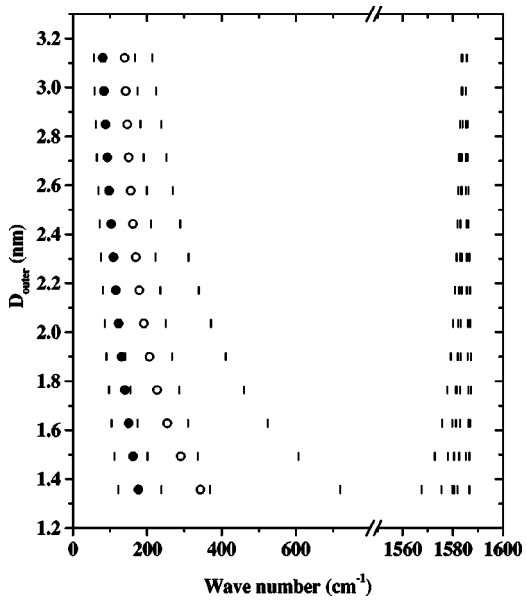

FIG. 2. Diameter dependence of the Raman-active mode frequencies for $(n,n)@(n+5,n+5)$ DWCNT's. Low-frequency RBLM's (solid circle) and high-frequency RBLM's (open circle).

A few years ago, in the framework of the bond-polarization theory, and using the spectral moment method, we found, in agreement with different approaches, that the diameter dependence of the RBM frequency in isolated SWCNT's was given by the relation (1), with $A \approx 225$ cm^{-1} nm.[13] A different behavior is found for both the RBLM's in DWCNT's. In the diameter range of inner tubes, 0.6–2.4 nm, the frequency shift of the highest-frequency RBLM's (counterphase vibrations of both tubes) with respect to the position of the RBM's of the isolated inner tube is found to depend linearly on the inner tube diameter (Fig. 3). In contrast, in the related diameter range of the outer tubes: 1.2–3 nm, we found that the shift of the low-frequency RBLM's (in-phase motions of both tubes) with respect to the RBM frequency of the isolated outer tube is no longer linear (Fig. 3). For very small diameters, the shift is linear.[22] The change in the shift behavior occurs around 1.7 nm. It is related to an increase of the interaction between the tubes. Indeed, as discussed in Ref. 21, for the small diameters, each of the two RBLM's has the characteristic features of the RBM of one of the tube. In contrast, for large diameter (above 1.7 nm in our work), the low- and high-frequency RBLM's are in-phase and counterphase collective motions of both tubes, respectively. The dependencies of the RBLM frequencies as a function of the diameter (Figs. 2 and 3) are close to those found in recent and different approaches (see, for instance, Fig. 4 in Ref. 21 and Fig. 3 in Ref. 22).

The position of the high-frequency RBLM, ω_{HF}, is well fitted by the analytical expression

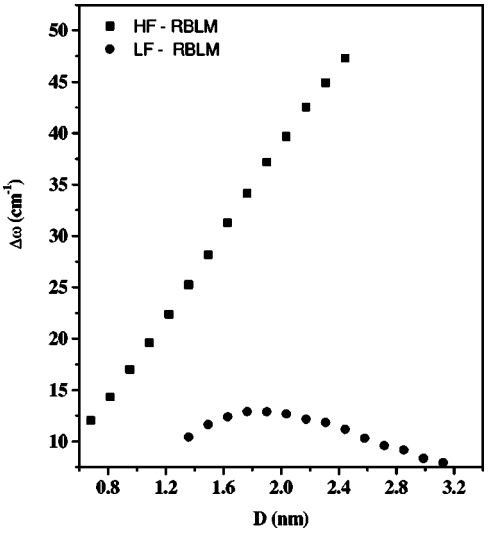

FIG. 3. Dependence of the gap between RBLM and RBM as a function of the tube diameter for $(n,n)@(n+5,n+5)$ DWCNT's. High-frequency RBLM's (solid square) and low-frequency RBLM's (solid circle).

$$\omega_{HF}(\mathrm{cm}^{-1}) = \frac{A_i}{D_{inner}} + B_i D_{inner} + C_i \qquad (2)$$

with parameters close to $A_i = 225\ \mathrm{cm}^{-1}\,\mathrm{nm}$, $B_i = 20.6\ \mathrm{cm}^{-1}\,\mathrm{nm}^{-1}$, $C_i = -2.4\ \mathrm{cm}^{-1}$. On the other hand, the dependence of the position of the RBLM's of lowest frequency, ω_{LF}, is well fitted by the relation

$$\omega_{LF}(\mathrm{cm}^{-1}) = \frac{A_o}{D_{outer}^2} + \frac{B_o}{D_{outer}} + C_o \qquad (3)$$

with parameters close to $A_o = -88.8\ \mathrm{cm}^{-1}\,\mathrm{nm}^2$, $B_o = 324.1\ \mathrm{cm}^{-1}\,\mathrm{nm}$, $C_o = -14.7\ \mathrm{cm}^{-1}$.

It must be emphasized that these previous expressions only have a useful interest to relate the diameter of tubes and the experimental RBLM frequencies. No physical meaning is attached to the values of the different parameters of the fit.

Focusing now on the TLM range of $(n,n)@(n+5,n+5)$ DWCNT's, we find that the Raman spectrum displays six modes associated with the in-phase and counterphase coupled motions of the tangential modes (TM's) of the inner and outer tubes. As previously, we identify the TLM's from the symmetry of the parent TM's of the inner and outer tubes. For example, the calculated Raman spectrum of the (7,7)@(12,12) DWCNT's displays TLM's at 1580 and 1583 cm^{-1} (A_{1g}), 1575 and 1581 cm^{-1} (E_{1g}), 1587 and 1586 cm^{-1} (E_{2g}), resulting from the coupling of the A_{1g}, E_{1g}, and E_{2g} modes of the (7,7) inner tube and (12,12) outer tube, respectively. The position of the TLM as a function of the diameter of the outer tube, D_{outer}, is plotted in Fig. 2. When the tube diameter increases, an upshift of the A_{1g} and E_{1g} TLM's and a slight downshift of the E_{2g} TLM's are predicted. In consequence, an unresolved broad TLM band is expected around 1582 cm^{-1} in the calculated Raman spectrum of DWCNT's of large diameter.

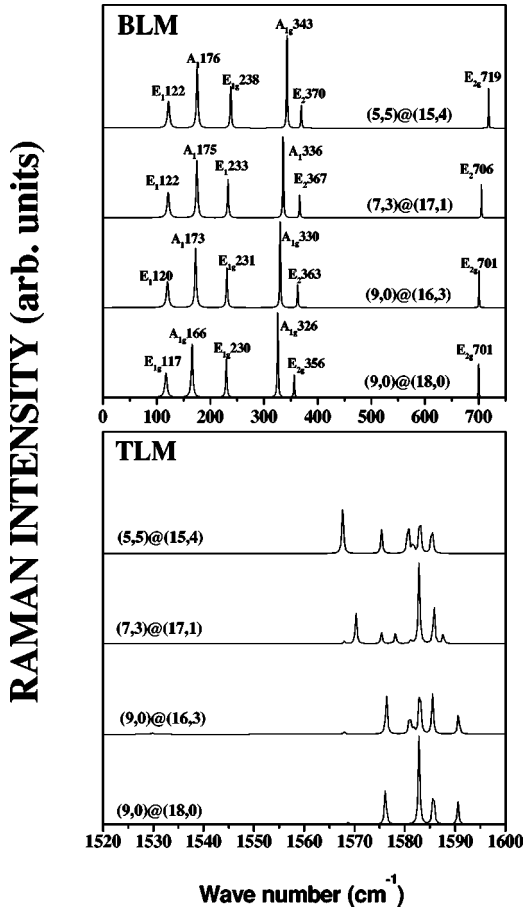

FIG. 4. The calculated Raman spectra of (9,0)@(18,0), (9,0)@(16,3), (7,3)@(17,1), and (5,5)@(15,4) DWCNT's in the BLM (top) and TLM (bottom) regions.

The Raman spectrum of zigzag@zigzag DWCNT's have also been calculated. With the tube-tube separation being assumed to be close to 3.4 Å, we found that the $(n,0)@(n+9,0)$ DWCNT satisfies this condition ($d \approx 3.55$ Å). Note that this separation distance is slightly larger than that in the $(n,n)@(n+5,n+5)$ DWCNT ($d \approx 3.4$ Å). Finally, for DWCNT's containing a chiral tube, we consider all the combinations with a tube-tube distance located in the 3.4–3.55 Å range.

For tubes of close diameters, we found that the BLM regions of the Raman spectra of armchair@armchair, zigzag@zigzag, armchair@chiral, and zigzag@chiral DWCNT's are similar. This means that, as in SWCNT, the BLM's are not significantly dependent on the chirality of the tube. By contrast, the Raman spectrum in the TLM region is very sensitive to the chirality of the tubes. To illustrate these results, we report in Fig. 4 the Raman spectra in the BLM and TLM regions calculated for different kinds of DWCNT's with close diameters: $D_{inner} \approx 0.7$ nm for the inner tube and $D_{outer} \approx 1.4$ nm for the outer tube. The similarity of the spectra in the BLM region can be pointed out. By contrast, it can be emphasized that the number of modes in the TLM range is very sensitive to the chirality of the tubes. This leads to a chirality dependence of the profile and average frequency of the TLM bunch.

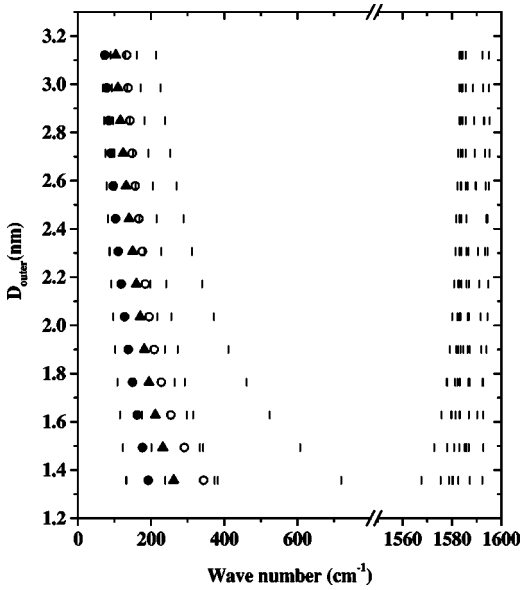

FIG. 5. Diameter dependence of the Raman-active mode frequencies for $(n,n)@(n+5,n+5)$ DWCNT crystals. Low-frequency RBLM's (solid circle), high-frequency RBLM's (open circle), BBLM's (solid triangle).

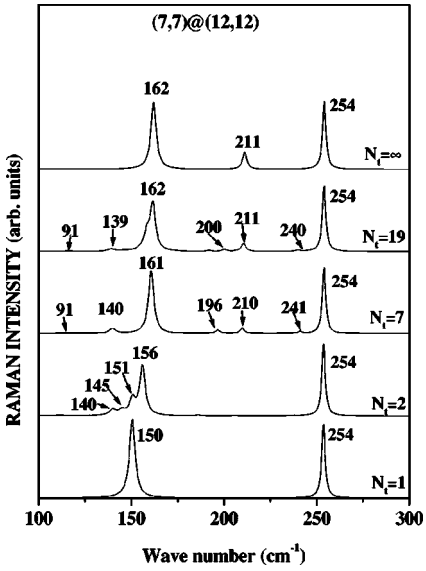

FIG. 6. Dependence of the RBLM range of (7,7)@(12,12) DWCNT's as a function of the number of tubes in the bundle. N_t=1, 2, 7, 19, infinity.

The behavior of the Raman spectrum with the length of the tube has also been analyzed. For DWCNT lengths smaller than 40 nm, a large number of additional peaks are observed in the Raman spectrum, especially in the BLM range. The intensity of these peaks rapidly decreases when the length of the tube increases. For a length of about 40 nm the position and intensity of the peaks are very close to those calculated for DWCNT's of infinite length. In consequence, the effect of the tube length on the Raman spectrum could be only observed experimentally on very small tubes. Because in the majority of the experiments, DWCNT's are longer than 40 nm, our calculations for the infinite tubes can be used to interpret the Raman experiments on DWCNT samples.

B. The Raman spectrum of DWCNT bundle

The Raman spectra of crystals of armchair@armchair $[(n,n)@(n+5,n+5)]$ DWCNT's (bundle of infinite size) have been calculated. The dependence of the frequencies of Raman modes with the diameter of the outer tube is displayed in Fig. 5. Comparison between the Raman spectra of isolated DWCNT and DWCNT crystals shows no significant difference in the TLM region, except a slight upshift of the TLM in the DWCNT crystal. By contrast, in the BLM range, new modes appear in the DWCNT crystal. In order to identify some of these specific modes, we focus on the polarized *ZZ* Raman spectrum of the DWCNT crystal. Indeed, it was previously found in SWCNT's that the intensity of the $A_{1g}(A_1)$ RBM's in the *ZZ* spectrum is weak but not equal to zero, in contrast with those of the breathing modes of $E_{1g}(E_1)$ and $E_{2g}(E_2)$ symmetries, which are nonactive in this polarized spectrum. Three Raman modes dominate the *ZZ* spectrum, the two expected RBLM's and an additional mode located between the two RBLM's, labeled BBLM (for bundle breathing-like mode) in the following. The intensity of this latter mode increases with increasing diameter of the tubes. In order to illustrate this result, the calculated polarized *ZZ* Raman spectrum of a crystal of (7,7)@(12,12) DWCNT is displayed in Fig. 6 (top curve). The RBLM of the lowest frequency is upshifted by about 12 cm^{-1} with respect to its position for isolated DWCNT's (Fig. 6, bottom curve). By contrast, the RBLM of the highest frequency is at the same position in isolated DWCNT's and DWCNT crystals. The additional BBLM is located at 211 cm^{-1}. As in isolated DWCNT's, the diameter dependence of the frequencies of these modes (Fig. 5) can be approximated by different expressions. Because the RBLM of the highest frequency is not affected by DWCNT-DWCNT interactions, its frequency, ω_{HF}, is given by the same expression than for isolated tube [expression (2)]. On the other hand, the diameter dependence of the RBLM of the lowest frequency, ω_{LF}, is given by expression (3) with parameters close to $A_o=-117$ cm^{-1} nm^2, $B_o=407$ cm^{-1} nm, $C_o=-44.5$ cm^{-1}. Also, the diameter dependence of the BBLM is well described by the relation:

$$\omega_{BBLM}(\mathrm{cm}^{-1}) = \frac{A_{BM}}{D_{outer}} - C_{BM} \tag{4}$$

with $A_{BBLM}=378$ cm^{-1} nm and $C_{BBLM}=16.5$ cm^{-1}. It must be remembered that these different expressions only have a useful interest to relate the diameter of tubes and the experimental frequency in the BLM range.

Finally, we are interested with the dependence of the Raman spectrum on the number of tubes in the bundle. By contrast with the significant dependence of the spectrum in the low-frequency range to the size of the bundle, we found

TABLE I. Estimated inner and outer diameters (in nm) and their corresponding frequencies (in cm^{-1}) calculated from Eqs. (2) and (3) (ω^S is given from the linear relationship $\omega^S = 225.1/D$). The experimental frequencies, ω^{in}_{expt}, are those given in Refs. 15, 14, and 25.

Excitation	ω^{in}_{expt}	D_{in}	ω^{cal}_{out}	D_{out}	ω^{expt}_{out}	ω^{S}_{out}	ω^{S}_{in}
488 nm[a]	302	7.81	166	14.59	167	154	288
488 nm[b]	304	7.75	166	14.53	162	155	290
	384	6.02	184	12.81	182	176	374
514 nm[b]	267	8.97	155	15.78	150	143	251
	321	7.30	171	14.09	172	160	308
	385	6.00	185	12.79	185	176	375
488 nm[c]	265	9.05	155	15.84	150	142	249
	313	7.50	169	14.29	166	158	300
	330	7.08	173	13.87	175	162	318

[a]Reference 15.
[b]Reference 14.
[c]Reference 25.

that the TLM range slightly depends on the number of tubes per bundle. Focusing on the low-frequency range, we state that additional Raman modes appear in DWCNT bundles of small sizes. The intensity of the majority of these lines rapidly decreases with increasing the size of the bundle, except the BBLM, which subsists in the DWCNT crystal. The position of the low-frequency RBLM, ω_{LF}, monotonically upshifts when the number of tubes in the bundle increases. By contrast, the position of the highest-frequency RBLM, ω_{HF}, does not depend on the number of tubes in the bundle. Such a dependence of the Raman spectrum is shown in Fig. 6 for (7,7)@(12,12) bundles of different sizes. The number of tubes, N_t, is 2, 7, and 19, respectively. The polarized *ZZ* Raman spectra are compared with those calculated for isolated DWCNT's (Fig. 6, bottom) and crystals of DWCNT (Fig. 6, top). A first series of additional peaks appears on the low-frequency side of the low-frequency RBLM's. They are pointed at 140, 145, 151 cm^{-1} for $N_t=2$. When the number of tubes increases, these peaks shift, overlap, decrease in intensity, and vanish in DWCNT crystals. For $N_t>2$, a second series of additional peaks appears in the BM range. These peaks are located at 196, 211, and 240 cm^{-1} for $N_t=7$. The majority of these peaks disappear with increasing N_t, and finally only the BBLM located at 211 cm^{-1} remains for large N_t, and in DWCNT crystals.

IV. CONCLUSION

In Table I we compare the predictions of our model with the experimental RBLM's measured in Refs. 14, 15, and 25. From the experimental ω_{HF} we derive D_{inner} by using Eq. (2). D_{outer} is given by the usual expression $D_{outer}=D_{inner}+2d$. By using Eq. (3) we obtain a value of d. This value gives the best agreement between experimental and calculated ω_{LF}. It has to be reminded that d must be close of 3.4 nm, and the related D_{outer} diameter must be compatible with the assumed chirality of the outer tube.

General good agreement is found between predictions and experimental values (Table I). Focusing on the data obtained in our group,[25] we found that the Raman spectrum is dominated by six peaks around 150, 166, 175, 265, 313, and 330 cm^{-1}. From our calculations, we assign these peaks to three single DWCNT's: 9.04–15.9 Å, 7.47–14.36 Å, and 6.97–13.73 Å. From these values, a possible attribution of the DWCNT's can be proposed, for instance, (9,4)@(18,4), (6,5)@(16,4), and (7,3)@(17,1) DWCNT's, respectively. However, other DWCNT's can be compatible with the same experimental data. For instance, the calculations of the RBLM frequencies of (9,0)@(16,3) DWCNT's also predict peaks located around 173 and 330 cm^{-1}, close to the experimental data. In summary, the agreement between experimental and calculated RBLM frequencies (Table I) validates our approach and allows us to relate properly the RBLM frequency and the inner (outer) tube diameter in DWCNT's.

In conclusion, we have calculated the nonresonant Raman spectrum of isolated DWCNT's, and bundles of DWCNT's. The dependence of the spectrum with the diameter and the chirality of the inner and outer tubes of isolated DWCNT have been analyzed. Expressions are derived to describe the dependence with the diameter of the RBLM's in isolated infinite DWCNT's. These expressions can be used to experimentally derive the inner and outer tube diameters from the measurement of the RBLM frequencies. These expressions are valid for tubes longer than 40 nm, and they can be used to interpret the majority of the experiments on DWCNT's. For DWCNT bundles, we find that the low-frequency RBLM is significantly upshifted with respect to its position for isolated DWCNT's. Finally, a specific breathing-like mode is observed in DWCNT bundles.

ACKNOWLEDGMENTS

The computations were performed at CINES (Montpellier, France) on an SP2 IBM computer. The work was supported by a CNRS-France/CNCPRST-Morocco agreement.

*Also at Groupe de Dynamique des Phases Condensées (UMR CNRS 5581), Université Montpellier II, 34095 Montpellier Cedex 5, France

[1] T. Sugai, H. Omote, S. Bandow, N. Tanaka, and H. Shinohara, J. Chem. Phys. **112**, 6000 (2000).

[2] E. Flahaut, A. Peigney, Ch. Laurent, A. Rousset, J. Mater. Chem. **10**, 249 (2000).

[3] H. Zhu, C. Xu, B. Wei, and D. Wu, Carbon **40**, 2021 (2002).

[4] S. Bandow, G. Chen, G. U. Sumanasekera, R. Gupta, M. Yudasaka, S. Iijima, and P. C. Eklund, Chem. Phys. Lett. **337**, 48 (2001).

[5] M. S. Dresselhaus and P. C. Eklund, Adv. Phys. **49**, 705 (2000).

[6] J. L. Sauvajol, E. Anglaret, S. Rols, and L. Alvarez, Carbon **40**, 1697 (2002).

[7] M. S. Dresselhaus, G. Dresselhaus, A. Jorio, A. G. Souza Filho, and R. Saito, Carbon **40**, 2043 (2002).

[8] A. M. Rao, E. Richter, S. Bandow, B. Chase, P. C. Eklund, K. A. Williams, S. Fang, K. R. Subbaswamy, M. Menon, A. Thess, R. E. Smalley, G. Dresselhaus, and M. S. Dresslhaus, Science **275**, 187 (1997).

[9] R. Saito, T. Takeya, T. Kimura, G. Dresselhaus, and M. S. Dresselhaus, Phys. Rev. B **57**, 4145 (1998).

[10] J. Kürti, G. Kresse, and H. Kuzmany, Phys. Rev. B **58**, R8869 (1998).

[11] D. Sánchez-Portal, E. Artacho, J. M. Soler, A. Rubio, and P. Ordejón, Phys. Rev. B **59**, 12 678 (1999).

[12] G. D. Mahan, Phys. Rev. B **59**, 10 928 (1999).

[13] A. Rahmani, J. L. Sauvajol, S. Rols, and C. Benoit, Phys. Rev. B **66**, 125404 (2002).

[14] S. Bandow, M. Takizawa, H. Hirahara, M. Yudasaka, and S. Iijima, Phys. Rev. B **66**, 075416 (2002).

[15] R. Bacsa, A. Peigney, C. Laurent, P. Puech, and W. S. Bacsa, Phys. Rev. B **65**, 161404(R) (2002).

[16] L. Ci, Z. Zhou, X. Yan, D. Liu, H. Yuan, L. Song, J. Wang, Y. Gao, J. Zhou, W. Zhou, G. Wang, and S. Xie, J. Phys. Chem. B **107**, 8760 (2003).

[17] S. Rols, A. Righi, L. Alvarez, E. Anglaret, R. Almairac, C. Journet, P. Bernier, J. L. Sauvajol, A. M. Benito, W. K. Maser, E. Muñoz, M. T. Martinez, G. F. de la Fuente, A. Girard, and J. C Ameline, Eur. Phys. J. B **18**, 201 (2000).

[18] D. Kahn and J. P. Liu, Phys. Rev. B **60**, 6535 (1999).

[19] L. Henrard, E. Hernández, P. Bernier, and A. Rubio, Phys. Rev. B **60**, R8521 (1999).

[20] V. N. Popov and L. Henrard, Phys. Rev. B **63**, 233407 (2001).

[21] V. N. Popov and L. Henrard, Phys. Rev. B **65**, 235415 (2002).

[22] E. Dobardžic, J. Maultzsch, I. Miloševic, C. Thomsen, and M. Damnjanovic, Phys. Status Solidi B **237**, R7 (2003).

[23] C. Benoit, E. Royer, and G. Poussigue, J. Phys.: Condens. Matter **4**, 3125 (1992).

[24] S Guha, J. Menendez, J. B. Page, and G. B. Adams, Phys. Rev. B **53**, 13 106 (1996).

[25] J. Cambedouzou, J.-L. Sauvajol, A. Rahmani, E. Flahaut, A. Peigney, and C. Laurent, Phys. Rev. B **69**, 235422 (2004).